Available online at www.sciencedirect.com
ScienceDirect
Metabolism Clinical and Experimental 57 (2008) 903–910
Metabolism
Clinical and Experimental
www.metabolismjournal.com

Iron inhibits hydroxyapatite crystal growth in vitro

Pascal Guggenbuhl[a,b], Robert Filmon[a], Guillaume Mabilleau[a], Michel F. Baslé[a], Daniel Chappard[a,*]

[a]*INSERM, U 922-LHEA, Faculté de Médecine, Angers Cédex 49045, France*
[b]*Service de Rhumatologie, Hôpital Sud, CHU, Rennes Cédex 2 35203, France*

Received 1 December 2006; accepted 23 February 2008

Abstract

Hemochromatosis is a known cause of osteoporosis in which the pathophysiology of bone loss is largely unknown and the role of iron remains questionable. We have investigated the effects of iron on the growth of hydroxyapatite crystals in vitro on carboxymethylated poly(2-hydroxyethyl methacrylate) pellets. This noncellular and enzyme-independent model mimics the calcification of woven bone (composed of calcospherites made of hydroxyapatite crystals). Polymer pellets were incubated with body fluid containing iron at increasing concentrations (20, 40, 60 μmol/L). Hydroxyapatite growth was studied by chemical analysis, scanning electron microscopy, and Raman microscopy. When incubated in body fluid containing iron, significant differences were observed with control pellets. Iron was detected at a concentration of 5.41- to 7.16-fold that of controls. In pellets incubated with iron, there was a ~3- to 4-fold decrease of Ca and P and a ~1.3- to 1.4-fold increase in the Ca/P ratio. There was no significant difference among the iron groups of pellets, but a trend to a decrease of Ca with the increase of iron concentration was noted. Calcospherite diameters were significantly lower on pellets incubated with iron. Raman microspectroscopy showed a decrease in crystallinity (measured by the full width of the half height of the 960 Δcm^{-1} band) with a significant increase in carbonate substitution (measured by the intensity ratio of 1071 to 960 Δcm^{-1} band). Energy dispersive x-ray analysis identified iron in the calcospherites. In vitro, iron is capable to inhibit bone crystal growth with significant changes in crystallinity and carbonate substitution.

1. Introduction

Iron is a vital element for the survival of animals, plants, and microorganisms [1]. Because of its capacity to accept and donate electrons readily (converting Fe^{3+} in Fe^{2+}), it is a useful component of cytochromes, oxygen-binding molecules (eg, hemoglobin and myoglobin) and enzymes [2]. In genetic hemochromatosis (mostly due to HFE C282Y homozygote gene mutation), iron overload can lead to severe complications as nonalcoholic cirrhosis with liver adenocarcinoma, congestive heart failure, diabetes, sexual impotence, joint damages, and bone loss [3]. Severe complications of the disease can be now prevented by phlebotomia and, fortunately, most of the patients do not die anymore from the disease itself. In this context of chronic disease, the impact of iron overload on bone metabolism was described only recently. Osteoporosis occurs in 29% to 34.2% of patients in recent series [4,5] and the risk of vertebral fracture can reach 20% [6]. In former studies, it was hypothesized that hypogonadism, cirrhosis, low vitamin D levels [6], or hyperparathyroidism [7] could be responsible for bone loss. However, these patients had a very severe form of hemochromatosis and did not fulfill the actual standards for bone evaluation. Recently, it has been found in an homogeneous male population with the HFE C282Y homozygote mutation, that none of these factors could solely explain osteoporosis in genetic hemochromatosis [4]. Little is known about the pathophysiologic mechanisms leading to osteoporosis in genetic hemochromatosis. Classic risk factors (particularly hypogonadism) can participate to bone loss but do not appear to play the key role. The direct

* Corresponding author. Tel.: +33 241 73 58 65; fax: +33 241 73 58 86.
E-mail address: daniel.chappard@univ-angers.fr (D. Chappard).

0026-0495/$ – see front matter © 2008 Elsevier Inc. All rights reserved.
doi:10.1016/j.metabol.2008.02.004

pathological effect of Fe^{3+} at the tissue level has been seldom considered. Iron overload has been found on bone biopsy in patients with hemochromatosis. Positive iron staining of osteoblasts, osteoclasts, and bone matrix is observed in patients [8,9] and confirmed by animal studies [10,11]. Histomorphometric studies of iron-overloaded bone have essentially shown a decrease in bone formation and an occasional increase in bone resorption in patients with associated hypogonadism. Osteomalacia has never been found in patients [12-14]. Why hemochromatosis leads to osteoporosis even in the absence of hypogonadism or liver complications is not fully understood.

In this study, we have investigated the role of iron on the in vitro growth of hydroxyapatite crystals. We used a modified polymer, carboxymethylated poly (2-hydroxyethyl methacrylate) (pHEMA-CM), which can mimic the calcification of woven bone [15]. Pellets of the polymer were incubated in a synthetic body fluid containing iron (Fe^{3+}) at increasing concentrations because Fe^{3+} is the circulating form of iron in the blood and extracellular fluids [16,17]. The hydroxyapatite growth in presence of iron was studied by chemical analysis, scanning electron microscopy (SEM), and Raman microscopectroscopy.

2. Materials and methods

2.1. The monomer

Commercial 2-hydroxyethyl methacrylate (HEMA) was purchased from Sigma-Aldrich Chemical (Illkirsh, France). Commercial HEMA contains residual methacrylic acid and cross-linkers due to the fabrication process. The polymerization inhibitor 4-methoxyphenol (added by the manufacturer before shipping, at a concentration of 350 ppm) also needs to be removed. HEMA was purified and distilled under reduced pressure (5×10^{-2} mBar, 70°C).

2.2. Preparation of the polymer

The linear polymer was prepared by bulk polymerization. Briefly, the polymerization mixture was composed of HEMA (10 mL) and 0.2 g of benzoyl peroxide (BPO) used as initiator. The mixture was accelerated by *N*,*N*-dimethyl-*para*-toluidine in a molar ratio of benzoyl peroxide to *N*,*N*-dimethyl-*para*-toluidine of 100:1 (mol/mol). Monomers were polymerized at 4°C for 2 hours in polypropylene wells (Delta Microscopies, Labege, France). In that way, calibrated pellets of pHEMA were obtained (150 ± 5 mg) with a great regularity. Carboxymethylation of the pellets was done by the modified method of Garrett et al [18]. Briefly, the pellets were washed with deionized water (USF ELGA, Purelab Plus, Ransbach-Baumbach, Germany) for 30 minutes and soaked in 0.5 mol bromoacetic acid in a 2-mol NaOH solution for 18 hours at room temperature, under gentle agitation. Pellets of the carboxymethylated polymer (pHEMA-CM) were washed 3 times (10 min each) in deionized water.

2.2.1. Incubation of pellets in synthetic body fluid

A standard synthetic body fluid (medium-1×) mimicking the lymph fluid was prepared according to Yamada et al [19]. Its composition (verified on a Technicon SMA analyzer, Emeryville, CA) was as follows: Na, 142.19 mmol/L; Ca, 2.49 mmol/L; Mg, 1.5 mmol/L; HCO_3, 4.2 mmol/L; Cl, 141.54 mmol/L; HPO_4, 0.9 mmol/L; SO_4, 0.5 mmol/L; K, 4.85 mmol/L. Pellets of pHEMA-CM materials were sterilized by UV radiation (360 nm for 3 hours) and were distributed in sterile-capped vials containing 50 mL of the synthetic medium (1.25×) during 5 days at 37°C to induce the appearance of hydroxyapatite globules (calcospherites) at their surface. The pellets were transferred into an enriched body fluid (medium-1.25×) containing 0, 20, 40 or 60 μmol/L iron (Fe^{3+}) during 12 days. The groups incubated with Fe supplemented body fluid will be referred as the "iron groups" I20, I40, and I60, and the pellets incubated without iron will constitute the control group. Pellets were soaked in a humidified oven at +37°C, with an inflowing air containing 5 vol% CO_2. The fluid was replaced every 2 days. At the end of the incubation period, the pellets were rinsed in deionized water for 3 × 10 minutes to remove the noncrystallized ions. Twelve pellets were incubated for each period and for each iron concentration, so the following analyses were done in triplicate.

2.3. Chemical analysis

Transfer of the pellets in HCl 0.2 mol (1 mL) for 24 hours led to a complete dissolution of calcospherites. The fluid was then collected and used to determine the amount of free ions on an automated biochemistry Hitachi 917 spectrophotometer (Roche, France) with standardized clinical reagents for iron (FerroZine Iron), calcium (Calcium Infinity Arsenazo III), and phosphate (reduced phosphomolybdate method) [20] obtained from the manufacturer. Measurement was performed on the fluid obtained from 3 pellets incubated in the same conditions, and the mean ± SD of the triplicate was considered.

2.4. Scanning electron microscopy and energy-dispersive x-ray analysis

Pellets to be examined by SEM, were processed as previously described [21]. Briefly, pellets whose surface was covered by calcospherites were dehydrated and carbon-coated (10 nm thick) with a MED 020 (Bal-Tec, Balzers, Liechtenstein). Scanning electron microscopy was performed on a JEOL 6301F (Jeol-France, Paris) field emission microscope equipped with an energy dispersive x-ray microanalysis machine (EDX, Link ISIS, Oxford Instruments, Oxford, UK). EDX was done by point analysis at the surface of calcospherites to determine their composition; the method explores several micrometers in thickness [22]. To illustrate the areas of iron deposition, 3 pellets covered by calcospherites incubated in body fluid containing Fe^{3+} were embedded in methyl methacrylate. They were fractured transversally in liquid nitrogen to expose the pHEMA and the layer of calcospherites. EDX analysis was done by line scanning: it is

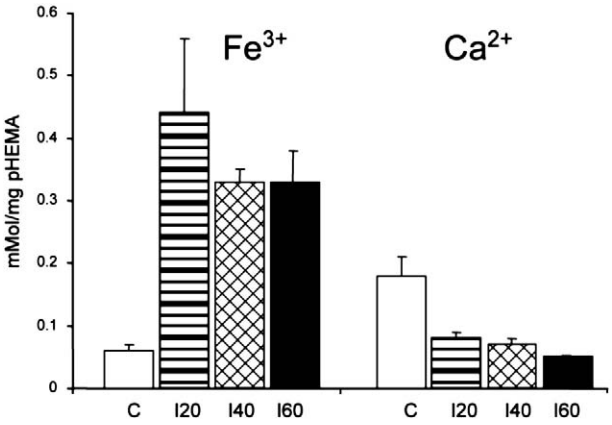

Fig. 1. Fe^{3+} and Ca concentration (mMP/mg polymer) in pHEMA-CM pellets incubated with 1.25× body fluid with and without Fe: controls, 0; I20, 20 μmol/L; I40, 40 μmol/L; and I60, 60 μmol/L. Significant differences with controls (C) are detailed in Table 1.

a useful method for investigating the change in elements along a line of traverse on the specimen surface. Each pixel along the testing line is analyzed to provide its own spectrum of data for selected elements. The intensity of elements along the length of the testing line is plotted and corresponds to the distribution of Ca, P, and Fe from the surface of the polymer to the different layers of calcospherites.

2.5. Raman microspectroscopy

Raman analysis was performed on a Senterra microscope with the OPUS 5.5 software (BRUKER OPTIK, Ettlingen, Germany). The excitation laser wavelength was 785 nm. The long working distance of the 20× microscope objective gave a spot size in the order of a few micrometers. The Raman microspectroscopy consists in a continuous laser beam focused on a sample through a microscope. From photons interaction with the molecules of the sample, crystallographic and molecular group characteristics can be assessed. The final spectrum of each spot was the average of 4 scans. Automatic baseline correction removes residual fluorescent background, resulting in fluorescent-free spectra. Values from peak intensities and bandwidths of peak recorded spectrum were used as described in the literature using the vendor-supplied scripts [23]. Two bands were investigated: phosphate band (PO_4^{3-} symmetric stretch at 960 cm^{-1}) and carbonate band (CO_3^{2-} symmetric stretch at 1071 cm^{-1}). From these measurements, we calculated crystallinity (expressed in cm^{-1}) as the bandwidth at the half peak intensity of the PO_4^{3-} band at 960 cm^{-1} [24]. Crystallinity is improved as the mineral crystal size increases. In hydroxyapatite, the substitution of the PO_4^{3-} functional group by CO_3^{2-} is coined a type B carbonate substitution [24,25]. Carbonate substitution was calculated as the ratio of the intensity of the PO_4^{3-} peak at 960 cm^{-1} to the intensity of CO_3^{2-} peak at 1071 cm^{-1} [23,26]. Ten peaks of each band were analyzed for each sample. Although other forms of substitutions exist, only the bCO_3^{2-} substitution was investigated in this study. The extent of type B carbonate substitution was quantified by dividing bCO_3^{2-} intensity with the PO_4^{3-} intensity.

2.6. Statistical analysis

Data analysis was performed with the Statistical Package for Social Science 12.0.1 software (SPSS, Chicago, IL). Data are expressed as mean ± SD. The significance of differences between groups was calculated by analysis of variance procedure, and when a significant difference was found, Fisher least significant difference test for post hoc between group comparisons was used at the 95% significance level.

3. Results

3.1. Chemical composition of pellets

The pellets did not vary in shape or weight under standardized polymerization conditions. They were translucent, and their mean weight was 149 ± 4.3 mg without significant differences between groups. When incubated in 1.25× body fluid with iron, there were significant differences between the iron groups and controls for chemical analysis. As expected, the amount of Fe^{3+} was higher in the iron groups, but no significant difference could be evidenced between them. The mean Fe^{3+} concentration was 0.06 ± 0.01 mmol/L per milligram of pHEMA in the control pellets and 5.41- to 7.16-fold more in the iron groups ($P < .05$ and .01) (Fig. 1 and Table 1). There was a lower amount of Ca (Fig. 1) and P and a higher Ca/P ratio in the iron groups than in controls (Table 1). There was a dramatic decrease in P and Ca with, respectively, 2.9- to 4.4-fold and 2.12- to 3.27-fold

Table 1
Fe^{3+}, Ca^{2+}, and PO_4^{3-} concentrations in pHEMA-CM pellets incubated with 1.25× body fluid with Fe^{3+} (0, 20, 40, and 60 μmol/L)

Mean ± SD	Fe^{3+} (mmol/L per milligram of pHEMA)	PO_4^{3-} (mmol/L per milligram of pHEMA)	Ca^{2+} (mmol/L per milligram of pHEMA)	Ca^{2+}/ PO_4^{3-}
controls	0.06 ± 0.01	0.11 ± 0.02	0.18 ± 0, 03	1.58 ± 0.07
I20	0.44 ± 0.12 ***	0.04 ± 0.01 ***	0.08 ± 0.01	2.18 ± 0.28 *
I40	0.33 ± 0.02 **	0.04 ± 0.01 ***	0.07 ± 0.01 ***	2.01 ± 0.06 *
I60	0.33 ± 0.05 **	0.03 ± 0.001 ***	0.05 ± 0.003 ***	2.12 ± 0.12 **

* $P < .05$, significant difference with controls.
** $P < .01$, significant difference with controls.
*** $P < .0001$, significant difference with controls.

in iron groups vs controls and a 1.27- to 1.38-fold increase in the Ca/P ratio in irons groups vs controls. There was no significant difference for Ca and P between the iron groups but a trend to a decrease of Ca with the increase of iron concentration (Table 1 and Fig. 1).

3.2. Scanning electron microscopy

After incubation in the body fluid, a white mineral layer composed of mineralized nodules was clearly shown by SEM. Mineralized nodules had a rounded shape (calcospherites); they were made of elementary tablets or plates of hydroxyapatite, packed together as previously reported [27]. A significant difference was found in calcospherite diameter between controls (Fig. 2A) and iron groups (Fig. 2B). In the latter, the calcospherite diameter was significantly lower than controls (I20, 1.28 ± 0.35; I40, 1.15 ± 0.31; I60, 1.25 ± 0.41 μm and 2.34 ± 0.41 μm in controls; $P < .0001$). There was no difference for calcospherite size between the iron groups. On the EDX cartography, Ca, P, and Mg could be localized. Fe was only localized in the iron groups. There was no difference in Fe spectrum intensity between the iron groups

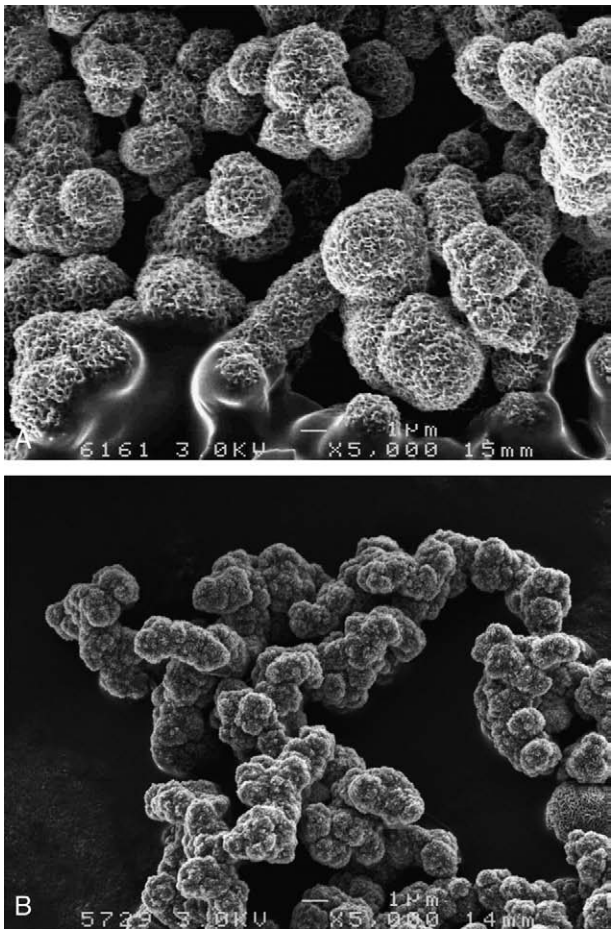

Fig. 2. A, SEM micrograph of a group of calcospherites incubated in body fluid without Fe^{3+} (control). B, A group of calcospherites incubated in body fluid with Fe^{3+}. Bar = 1 μm.

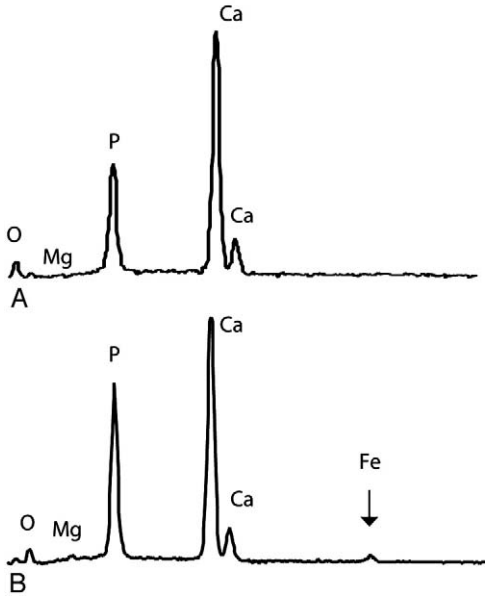

Fig. 3. EDX analysis of a control calcospherite (A) showing Ca, P, and Mg colocalization. The lower spectrum (B) is from an I40 calcospherite and the position of Fe is clearly illustrated.

(Fig. 3). On fractured pellets examined by line scanning in EDX (Fig. 4), the first band of calcospherites grown without iron was clearly identified (c). It is covered by the upper band containing calcospherites heavily and diffusely positive for iron (d).

3.3. Raman microspectroscopy

In Raman spectroscopic analysis, the physicochemical properties of calcospherites demonstrated significant changes between iron groups and controls (Fig. 5). The bandwidth at the half peak intensity of the PO_4^{3-} band, which is a reflection of crystallinity, was significantly lower in controls than in iron groups (except for I60 where the difference did not reach significance), suggesting a greater crystallinity in controls and a more ordered crystal lattice. The substitution of carbonate ions in phosphate positions given by the ratio of the intensity of the PO_4^{3-} peak to the intensity of CO_3^{2-} peak (reflecting the ratio phosphate/carbonate) was significantly greater in iron groups than in controls (13.5%-23.7%), suggesting a possible deterioration of structural mechanical properties as it was demonstrated previously [23] (Table 2).

4. Discussion

Iron is a vital trace element essential for cytochromes, oxygen-binding molecules, and enzymes. However, free iron can also damage tissues by producing free radical species as hydroxyl radical ($OH^{\bullet}$). Free radicals cause lipid peroxidation, changes in cell membranes composition and fluidity, and alteration of proteins and DNA, especially in case of iron

overload [28]. This has been well established in HIV infection, chronic hepatitis C, and alcoholism associated with increased iron concentrations [1,29]. Little is known about the relationships between iron and hydroxyapatite crystal, which is the most abundant constituent of bone mineral. In a study of iliac crest biopsies from 21 individuals with severe osteoporosis (at least one vertebral fracture), iron bone concentration (cortical and trabecular) was evaluated using inductively coupled plasma optical emission spectrometry. A significant increase in iron content in cortical bone was found in osteoporotic patients vs 12 controls. However, the authors thought that it was due to the increase of bone vascularization in more osteoporotic cortical bones, with an increase of red blood cells that can release iron [30]. Their data did not exclude abnormal iron absorption and a direct toxicity on bone.

Calcospherite growth on pHEMA-CM is a noncellular model mimicking the mineralization of woven bone. Woven bone is a peculiar bone texture observed in the growing skeleton, fracture callus, and metaplasia [31,32]. It has been developed to test drug efficacy (bisphosphonates) [32], cell adherence [31], and protein interaction during bone crystal growth [33]. In this study, we have used this model to evaluate the direct role of iron on bone mineralization. We found that Fe^{3+} induced a decrease in the calcospherite

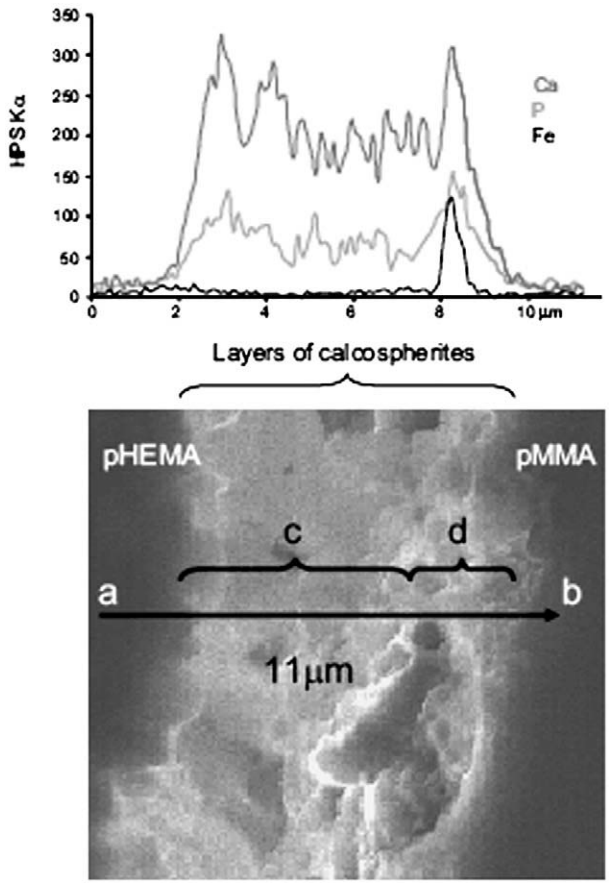

Fig. 4. EDX analysis of a pHEMA pellet embedded in methylmethacrylate and fractured. Line scanning of the sectioned thickness was done along the a-b line on a 10-μm length. Ca and P are clearly identified in the first layer (c), when calcospherites were grown without iron. Ca, P, and Fe are identified in the upper layer (d) and correspond to calcospherites that contain iron.

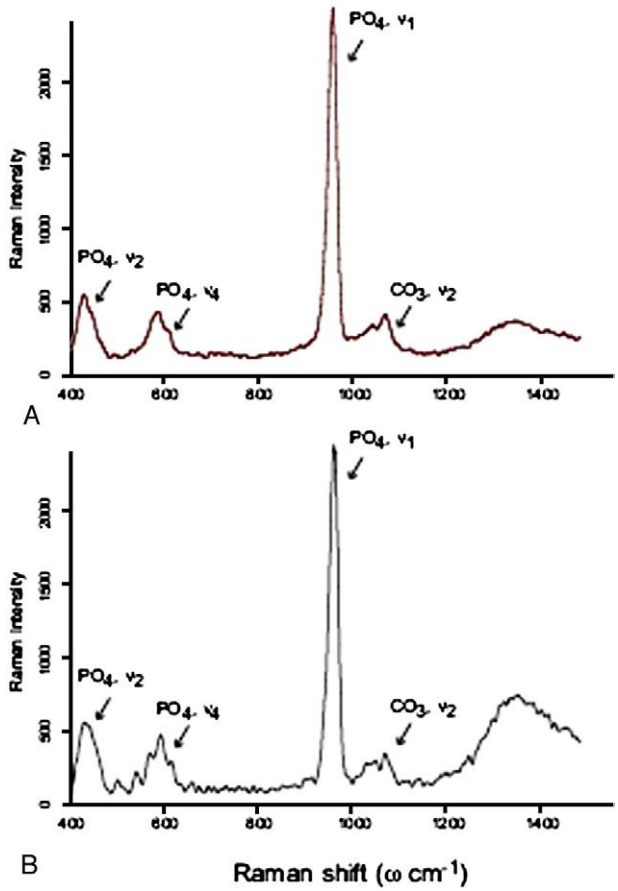

Fig. 5. Raman analysis of control calcospherites (A) and calcospherites from the I20 group (B) incubated in body fluid with Fe^{3+}. Note the difference in the carbonate bandwidth.

Table 2
Crystallinity and carbonate substitution values in pHEMA-CM pellets incubated with 1.25× body fluid with Fe^{3+} (0, 20, 40, and 60 μmol/L)

Mean ± SD	FWHH of 960 Δcm^{-1} band (cm^{-1})	Intensity ratio of 1071 to 960 Δcm^{-1} band
Controls	23.50 ± 0.34	9.85 ± 0.71
I20	24.22 ± 0.46 **, ‡	12.19 ± 1.46 ****
I40	24.86 ± 0.80 ***, †, §	11.18 ± 1.39 *
I60	23.77 ± 0.19	11.62 ± 1.01 ***

FWHH indicates full width of the half height and is a measure of relative degree of crystallinity. Intensity ratio of 1071 to 960 Δcm^{-1} band reflects differences in carbonate substitution.

* $P < .05$, CO_3^{2-}/PO_4^{3-} significant difference with controls.
** $P < .01$, CO_3^{2-}/PO_4^{3-} significant difference with controls.
*** $P < .001$, CO_3^{2-}/PO_4^{3-} significant difference with controls.
**** $P < .0001$, CO_3^{2-}/PO_4^{3-} significant difference with controls.
† $P < .01$, CO_3^{2-}/PO_4^{3-} significant difference with I20.
‡ $P < .01$, CO_3^{2-}/PO_4^{3-} significant difference with I40.
§ $P < .0001$, CO_3^{2-}/PO_4^{3-} significant difference with I60.

diameter and a dramatic decrease in Ca and P in the crystal content. This effect was independent of cellular or enzyme interactions because the model is acellular. There is a growing body of evidence that iron can play a deleterious role in bone. In genetic hemochromatosis, former human studies had found Perls blue staining in bone trabeculae of patients [8,9]. Furthermore, bone mineral density is decreased in patients with genetic hemochromatosis and severe iron overload [5], and a negative correlation has been found between hepatic iron concentration (a good index of total body iron overload) and bone mineral density at the femoral neck [4]. A study of overload with intramuscularly dextran iron was conducted during 36 days in pigs [10]; a linear deposit of iron inside the bone matrix was observed at the edge of the trabecular surfaces, at the osteoid/mineralized interface, and seldom in the cement lines. Iron was detected as large deposits in marrow macrophages, less frequently in osteoclasts or in osteoblasts. The main effect was a decrease in bone formation, without change in bone resorption or mineralization impairment. Osteopenia was induced in Sprague-Dawley rats fed a diet containing 50 000 ppm iron lactate (5%) for 2 or 4 weeks [34]. The bone volume, trabecular thickness, and trabecular number decreased without mineralization defect; surprisingly, no iron was found at the surface of the trabeculae. The bone formation (as assessed by osteocalcin and alkaline phosphatase dosages) and bone resorption (as assessed by urinary pyridinolin and deoxypyridinolin dosages) significantly increased vs controls; this was confirmed by bone histomorphometric parameter change. Parathyroid hormone levels decreased without iron deposits in parathyroid glands. Bone remodeling markers were approximately 30% lower after 4 weeks treatment than after 2 weeks. In this study, the reason why bone formation was increased despite low parathyroid hormone levels remains unclear. These results contrast with the changes seen in pigs treated with intramuscular dextran iron [10]. When the iron treatment lasted 13 weeks, positive iron bands were detected at the edge of all trabecular surfaces in the tibia and at the osteoid-mineralized bone interface. In this case, histology showed mineralization impairment similar to osteomalacia [35]. Recently, it was shown in old Wistar rats, fed iron lactate for 4 weeks, that reactive oxygen species accumulated in bone. Free radicals are released via the Fenton reaction in which Fe^{2+} produces $OH^{\bullet}$ in the presence of hydrogen peroxide. There was an increase in bone resorption markers (a 2.7-fold increase of urinary deoxypyridinolin than controls) and no change in bone formation markers. An iron lactate diet significantly decreased serum glutathione peroxidase enzyme activity, an enzyme that catalyzes the reduction of the oxidized glutathione, and an increase of urinary 8-hydroxy-2′-deoxyguanosine (8-OHdG), a marker of DNA oxidative damages.

In the present study, we found a direct effect of iron on the hydroxyapatite crystal with a decrease in the mean size of calcospherites and consequently a marked reduction in Ca/P deposit on the pHEMA-CM pellets. Fe^{3+} was diffusely incorporated in the calcospherites grown during the second step of the experiment (when iron was added in the body fluid) as shown by the line scanning analysis in EDX. It is known that iron can be incorporated into hydroxyapatite crystals in ectopic choroid plexuses and pineal gland calcifications [36] and in microshells made of calcium carbonate where it impairs mineralization [37]. The incorporation of large amounts of iron is also well known during the mineralization of the surface layers of dental enamel in practically all rodent incisors and in shrew molars [38]. Furthermore, iron is normally complexed with bone, dentine, and immature enamel as a postmortem artifact. Similarly, Fe^{2+} iron can be incorporated in calcite where it substitutes calcium and thus decreases mineralization rate [39]. It can be also incorporated in ceramics and biomaterials. In this study, iron was passively incorporated in hydroxyapatite with a decrease of crystal size without cellular, hormonal, or protein intervention. Moreover, Raman microspectroscopy showed an alteration of the crystal quality with a decrease of crystallinity and carbonate substitution in phosphates that could led to a bone strength decrease [23]. Scanning electron microscopy showed a direct toxic effect of iron on the crystal growth, a finding previously described by crystal modeling [40] and in synthetic hydroxyapatites [41]. Iron accumulation in patients with thalassemia or drepanocytosis is linked to the degree of osteopenia [42,43]. Fe^{3+} iron binds tightly phosphate groups and thus can affect the nature of the mineral precipitated, some studies showed that Fe^{3+} does not affect HA solubility [44]. The existence of metal trace elements in bone, such as aluminum or lead, is well known; however, the precise toxicity mechanisms remain largely unknown. In a human study on the effects of soluble metals on periimplant cells, a particulate precipitation was found at a Fe^{3+} concentration of 1 mmol/L (or higher) in the cell culture medium. This was associated with a 50% decrease in osteoblast proliferation at high concentration (10 mmol/L) [45]. Little is known about the exact biochemical composition of the periosteocytic fluid and the ratio to that of plasma has not been well studied. For example, it has been established that concentration of K^+ is much higher in the bone fluid than in plasma [46]. Here, iron concentrations near serum physiologic levels and a slightly higher were chosen. It is possible that local iron concentration in the bone fluid is higher. However, there was no difference on crystal growth and composition between the different iron concentrations, except for crystallinity, suggesting a saturation effect even at the smallest concentration used. It seemed that there was a dose effect and a saturation threshold as early as 20 mmol/L.

5. Conclusion

Iron inhibits growth and change quality of hydroxyapatite crystals in vitro, in an acellular and nonenzymatic model of

calcification. This suggests a direct effect of iron on bone mineralization and, consequently, on bone quality, independently of cells, proteins, and enzymes. Sexual hormones that had been designated as the only cause of osteoporosis in case of iron overload may not be the only cause because a direct toxic effect of the ion is evidenced in this in vitro study.

Acknowledgment

This work was made possible by grants from Contrat de Plan Etat-Region "Pays de la Loire," BIOREGOS (Biomatériaux et Régénération OsteoArticulaire, Nantes and Angers, France) INSERM (Institut national de la Santé et de la recherche médicale, Paris, France), and the Société Française de Rhumatologie (Paris, France).

References

[1] Arredondo M, Nunez MT. Iron and copper metabolism. Mol Aspects Med 2005;26:313-27.
[2] Emerit J, Beaumont C, Trivin F. Iron metabolism, free radicals, and oxidative injury. Biomed Pharmacother 2001;55:333-9.
[3] Brissot P, Le Lan C, Troadec MB, Lorho R, Ropert M, Lescoat G, et al. [HFE hemochromatosis: pathogenic and diagnostic approach]. Transfus Clin Biol 2005;12:77-82.
[4] Guggenbuhl P, Deugnier Y, Boisdet JF, Rolland Y, Perdriger A, Pawlotsky Y, et al. Bone mineral density in men with genetic hemochromatosis and HFE gene mutation. Osteoporos Int 2005;16: 1809-14.
[5] Sinigaglia L, Fargion S, Fracanzani AL, Binelli L, Battafarano N, Varenna M, et al. Bone and joint involvement in genetic hemochromatosis: role of cirrhosis and iron overload. J Rheumatol 1997;24: 1809-13.
[6] Diamond T, Stiel D, Posen S. Osteoporosis in hemochromatosis: iron excess, gonadal deficiency, or other factors? Ann Intern Med 1989; 110:430-6.
[7] Pawlotsky Y, Roussey M, Hany Y, Simon M, Bourel M. Increased blood parathormone levels in idiopathic hemochromatosis. Nouv Presse Med 1974;3:1757-8.
[8] Diamond T, Pojer R, Stiel D, Alfrey A, Posen S. Does iron affect osteoblast function? Studies in vitro and in patients with chronic liver disease. Calcif Tissue Int 1991;48:373-9.
[9] Duquenne M, Rohmer V, Legrand E, Chappard D, Wion Barbot N, Baslé MF, et al. Spontaneous multiple vertebral fractures revealed primary haemochromatosis. Osteoporos Int 1996;6:338-40.
[10] de Vernejoul MC, Pointillart A, Golenzer CC, Morieux C, Bielakoff J, Modrowski D, et al. Effects of iron overload on bone remodeling in pigs. Am J Pathol 1984;116:377-84.
[11] Ebina Y, Okada S, Hamazaki S, Toda Y, Midorikawa O. Impairment of bone formation with aluminum and ferric nitrilotriacetate complexes. Calcif Tissue Int 1991;48:28-36.
[12] Conte D, Caraceni MP, Duriez J, Mandelli C, Corghi E, Cesana M, et al. Bone involvement in primary hemochromatosis and alcoholic cirrhosis. Am J Gastroenterol 1989;84:1231-4.
[13] Diamond TH, Stiel D, Lunzer M, McDowall D, Eckstein RP, Posen S. Hepatic osteodystrophy. Static and dynamic bone histomorphometry and serum bone Gla-protein in 80 patients with chronic liver disease. Gastroenterology 1989;96:213-21.
[14] Pawlotsky Y, Lancien Y, Roudier G, Hany Y, Louboutin JY, Ferrand B, et al. Bone histomorphometry and osteo-articular manifestations of idiopathic hemochromatosis. Rev Rhum Mal Osteoartic 1979;46: 91-9.
[15] Filmon R, Grizon F, Baslé MF, Chappard D. Effects of negatively charged groups (carboxymethyl) on the calcification of poly(2-hydroxyethyl methacrylate). Biomaterials 2002;23:3053-9.
[16] Conrad ME, Umbreit JN. Pathways of iron absorption. Blood Cells Mol Dis 2002;29:336-55.
[17] Guggenbuhl P, Albert JD, Chales G. Rheumatic manifestations of genetic hemochromatosis. Presse Med 2007;36:1313-8.
[18] Garrett Q, Chatelier RC, Griesser HJ, Milthorpe BK. Effect of charged groups on the adsorption and penetration of proteins onto and into carboxymethylated poly(HEMA) hydrogels. Biomaterials 1998;19: 2175-86.
[19] Yamada S, Nakamura T, Kokubo T, Oka M, Yamamuro T. Osteoclastic resorption of apatite formed on apatite- and wollastonite-containing glass-ceramic by a simulated body fluid. J Biomed Mater Res 1994;28: 1357-63.
[20] Daly JA, Ertingshausen G. Direct method for determining inorganic phosphate in serum with the "CentrifiChem". Clin Chem 1972;18: 263-5.
[21] Filmon R, Chappard D, Baslé MF. Scanning and transmission electron microscopy of poly (2-hydroxyethyl methacrylate)-based biomaterials. J Histotechnol 1997;20:343-6.
[22] Newbury DE, Joy DC, Echlin P, Fiori CE, Goldstein J. Advanced Scanning Electron Microscopy and X-Ray Microanalysis. Springer; 1986.
[23] Akkus O, Adar F, Schaffler MB. Age-related changes in physicochemical properties of mineral crystals are related to impaired mechanical function of cortical bone. Bone 2004;34: 443-53.
[24] Paschalis EP, DiCarlo E, Betts F, Sherman P, Mendelsohn R, Boskey AL. FTIR microspectroscopic analysis of human osteonal bone. Calcif Tissue Int 1996;59:480-7.
[25] Akkus O, Polyakova-Akkus A, Adar F, Schaffler MB. Aging of microstructural compartments in human compact bone. J Bone Miner Res 2003;18:1012-9.
[26] Freeman JJ, Wopenka B, Silva MJ, Pasteris JD. Raman spectroscopic detection of changes in bioapatite in mouse femora as a function of age and in vitro fluoride treatment. Calcif Tissue Int 2001; 68:156-62.
[27] Filmon R, Chappard D, Monthéard JP, Baslé MF. A composite biomaterial: poly 2(hydroxyethyl) methacrylate/alkaline phosphatase (pHEMA/AlkP) initiates mineralization in vitro. Cells Mater 1996;6: 11-20.
[28] Garcia JJ, Martinez-Ballarin E, Millan-Plano S, Allue JL, Albendea C, Fuentes L, et al. Effects of trace elements on membrane fluidity. J Trace Elem Med Biol 2005;19:19-22.
[29] Puntarulo S. Iron, oxidative stress and human health. Mol Aspects Med 2005;26:299-312.
[30] Baslé MF, Mauras Y, Audran M, Clochon P, Rebel A, Allain P. Concentration of bone elements in osteoporosis. J Bone Miner Res 1990;5:41-7.
[31] Filmon R, Baslé MF, Atmani H, Chappard D. Adherence of osteoblast-like cells on calcospherites developed on a biomaterial combining poly (2-hydroxyethyl) methacrylate and alkaline phosphatase. Bone 2002; 30:152-8.
[32] Filmon R, Baslé MF, Barbier A, Chappard D. Poly(2-hydroxyethyl methacrylate)-alkaline phosphatase: a composite biomaterial allowing in vitro studies of bisphosphonates on the mineralization process. J Biomater Sci Polym Ed 2000;11:849-68.
[33] Filmon R, Cincu C, Baslé MF, Chappard D. Fetuin and osteocalcin influence calcospherite formation in an in vitro acellular model of calcification. Bone 2005;36:S2:171.
[34] Matsushima S, Hoshimoto M, Torii M, Ozaki K, Narama I. Iron lactate-induced osteopenia in male Sprague-Dawley rats. Toxicol Pathol 2001;29:623-9.
[35] Matsushima S, Torii M, Ozaki K, Narama I. Iron lactate-induced osteomalacia in association with osteoblast dynamics. Toxicol Pathol 2003;31:646-54.

[36] Alcolado JC, Moore IE, Weller RO. Calcification in the human choroid plexus, meningiomas and pineal gland. Neuropathol Appl Neurobiol 1986;12:235-50.
[37] Schulz KG, Zondervan I, Gerringa LJ, Timmermans KR, Veldhuis MJ, Riebesell U. Effect of trace metal availability on coccolithophorid calcification. Nature 2004;430:673-6.
[38] Selvig KA, Halse A. The ultrastructural localization of iron in rat incisor enamel. Scand J Dent Res 1975;83:88-95.
[39] Katz JL, Reick MR, Herzog RE, Parsiegla KI. Calcite growth inhibition by iron. Langmuir 1993;9:1423-30.
[40] Gutowska I, Machoy Z, Machalinski B. The role of bivalent metals in hydroxyapatite structures as revealed by molecular modeling with the HyperChem software. J Biomed Mater Res A 2005;75:788-93.
[41] Sutter B, Taylor RE, Hossner LR, Ming DW. Solid state 31phosphorus nuclear magnetic resonance of iron-, manganese-, and copper-containing synthetic hydroxyapatites. Soil Sci Soc Am J 2002;66: 455-63.
[42] Mahachoklertwattana P, Sirikulchayanonta V, Chuansumrit A, Karnsombat P, Choubtum L, Sriphrapradang A, et al. Bone histomorphometry in children and adolescents with beta-thalassemia disease: iron-associated focal osteomalacia. J Clin Endocrinol Metab 2003;88: 3966-72.
[43] Weinstein RS, Lutcher CL. Chronic erythroid hyperplasia and accelerated bone turnover. Metab Bone Dis Relat Res 1983;5:7-12.
[44] Christoffersen MR, Thyregod HC, Christoffersen J. Effects of aluminum(III), chromium(III), and iron(III) on the rate of dissolution of calcium hydroxyapatite crystals in the absence and presence of the chelating agent desferrioxamine. Calcif Tissue Int 1987;41: 27-30.
[45] Hallab NJ, Anderson S, Caicedo M, Brasher A, Mikecz K, Jacobs JJ. Effects of soluble metals on human peri-implant cells. J Biomed Mater Res A 2005;74:124-40.
[46] Knothe Tate ML. “Whither flows the fluid in bone?” An osteocyte’s perspective. J Biomech 2003;36:1409-24.